

EVOLUTION OF THE DUST PROPERTIES IN A TRANSLUCENT CLOUD

B. Stepnik^{1,2}, A. Abergel¹, J.-P. Bernard¹, F. Boulanger¹, L. Cambrésy^{3,4}, M. Giard², A. Jones¹, G. Lagache¹, J.-M. Lamarre¹, C. Meny², F. Pajot¹, F. Le Peintre¹, I. Ristorcelli², G. Serra², and J.-P. Torre⁵

¹Institut d'Astrophysique Spatiale (IAS), Bât. 121, Université Paris XI, F-91405 Orsay, France

²Centre d'Etude Spatial des Rayonnements (CESR), 9 av. Colonel Roche, BP 4346, F-31028 Toulouse, France

³Infrared Processing and Analysis Center (IPAC), California Institute of Technology, Mail Code 100-22, CA 91125, USA

⁴Département de Recherche Spatial (DESPA), Observatoire de Paris, F-92195 Meudon, France

⁵Service d'Aéronomie du CNRS (SA), BP 3, F-91371 Verrières Le Buisson, France

ABSTRACT

The balloon borne experiment PRONAOS/SPM has measured the submillimeter emission from 200 to 600 μm with an angular resolution of 2-3.5' of a quiescent translucent filament ($A_V \sim 4$) in the Taurus molecular complex. In order to analyse these data, we have developed a model for the emission of the filament using an independent tracer of the total column density (star count method on 2MASS stars) and a radiative transfer code. We first use in the model the optical properties of the dust from the standard model of Desert et al. (1990). The computed brightness profile fails to reproduce the data inside the filament. The agreement between data and model can only be obtained by changing the dust properties inside the filament. We have removed all particles not in thermal equilibrium from the densest part of the filament (typically $n_H \sim 10^4 \text{ cm}^{-3}$), and multiplied the submillimeter emissivity by a significant factor (~ 3). This suggests that grain-grain coagulation into fluffy aggregates occur inside the filament.

Key words: ISM: dust property, continuum emission – Missions: PRONAOS, FIRST – Object: Taurus complex

1. INTRODUCTION

It is now well established that the interstellar dust is made of several components differing in their chemical composition, structure and size. The smallest interstellar dust particles (sizes $\lesssim 15 \text{ nm}$) essentially emitting at wavelengths below 150 μm , are transiently heated in the InterStellar radiation Field (ISRF). The largest interstellar dust grains are in thermal equilibrium with the radiation field and their emission peaks around 100 μm (Desert et al. 1990). They have an average temperature of about 17.5 K in the diffuse atomic medium (Boulanger et al. 1996), with an emissivity similar to the value of the model of Draine & Lee (1984). However, this simple description does not take into account spatial variations of dust properties at small scale in our galaxy.

IRAS and COBE data indicate that there are spatial variations in the emitting properties of the interstellar

grains. IRAS data show that the colour of the dust emission in the ISM varies from place to place within the same molecular complex (Boulanger et al. 1990). In particular, the colour ratio $I_{60\mu\text{m}}/I_{100\mu\text{m}}$ can decrease dramatically from diffuse to molecular regions (Laureijs et al. 1991). This phenomenon is also observed in the Taurus molecular cloud (Abergel et al. 1994). The extended and diffuse part of the Taurus complex has a uniform IRAS colour ratio $I_{60\mu\text{m}}/I_{100\mu\text{m}}=0.15$. The dense and cold parts of the complex are filamentary structures (Abergel et al. 1994, Lagache et al. 1998), which present a deficit of 70-100% of its IRAS colour ratio $I_{60\mu\text{m}}/I_{100\mu\text{m}}$.

The physical properties of this cold dust is still not characterised because IRAS and COBE data do not combine the angular resolution and the spectral coverage required to analyse the thermal emission of individual clouds. However, PRONAOS/SPM, in combination with IRAS, constrains both the temperature and the emissivity spectral index of large grains at an angular resolution of 2-3.5'. These data allow us to better understand the origin and the nature of the cold dust in the ISM. This paper presents observations and analysis of one of these Taurus filaments.

2. OBSERVATIONS

2.1. PRONAOS/SPM INSTRUMENT

The observations have been performed with the PRONAOS experiment ('PROgramme National d'Astronomie Submillimétrique'). PRONAOS is a stratospheric balloon-borne which carry a two-meter telescope. SPM ('Spectro-Photomètre Multibande', see Lamarre et al. 1994), the focal instrument, is a single beam multi-band photometer. This instrument simultaneously performs measurements in four wide spectral bands, centred at 200, 260, 360 and 580 μm . The atmospheric residual emission is reduced using an oscillating mirror, which ensures a beam switching on the sky at a constant elevation. For this reason, PRONAOS/SPM is sensitive to emission gradients.

The photometric calibration is provided by ground measurements, two in flight black bodies, and planet observations. The final accuracy of this calibration is better than 10 % in absolute, and better than 5 % from channel to channel.

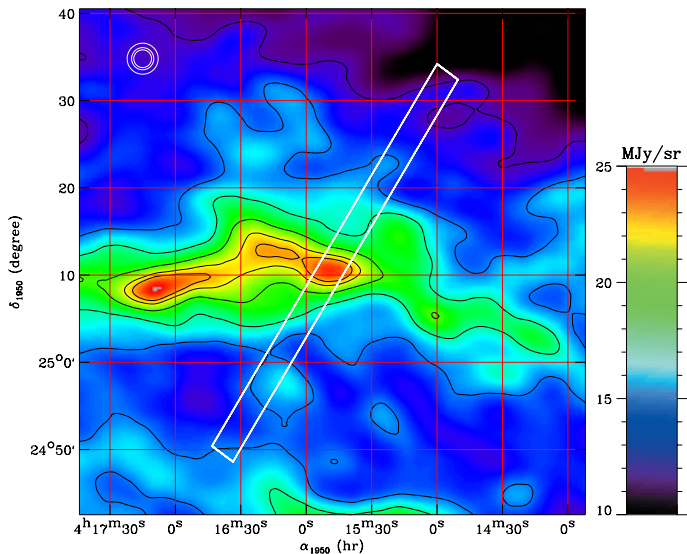


Figure 1. 100 μm IRAS map of the Taurus filament. The white box shows the region covered by the optical axis of PRONAOS/SPM (without including the instrument beam size). The PRONAOS/SPM beam sizes at each wavelength are shown by the circles on the top left side of the figure. The 100 μm IRAS contours are given from 11 to 23 MJy/sr with a step of 2 MJy/sr.

2.2. EMISSION PROFILES

The Taurus cloud observations were carried out during the second PRONAOS/SPM flight, on September 23rd 1996, from New-Mexico (USA). We have observed a map of $3' \times 50'$ centred at the position $\alpha_{1950} = 4^{\text{h}}15^{\text{m}}48^{\text{s}}$, $\delta_{1950} = 25^{\circ}12'01''$ (Fig. 1). To complement our data we have used HIRES (High RESolution processing) IRAS images of the cloud at 60 and 100 μm .

Black lines in Fig. 2a present the brightness profiles of the filament, averaged in a direction parallel to the long axis of the cloud, and degraded to the angular resolution of the 580 μm PRONAOS/SPM band (3.5'). The emission of the cloud can be separated into two components, a bright filament and a surrounding envelope. We have adjusted the surrounding envelope emission by a second order polynomial (green dashed lines in Fig. 2a).

2.3. TEMPERATURE PROFILES

We have modelled the cloud spectra using a single modified black body spectrum:

$$I_{\lambda}^{\text{fit}} = \epsilon_{250 \mu\text{m}} \cdot \left(\frac{\lambda}{250 \mu\text{m}} \right)^{-\beta} \cdot B_{\lambda}(T_{\text{dust}}),$$

where $\epsilon_{250 \mu\text{m}}$ is the dust emissivity at 250 μm , β the emissivity spectral index, and T_{dust} the dust temperature. The temperatures of the filament and the envelope are measured using PRONAOS/SPM data. The β value observed are always compatible with 2. Therefore, in the following, we set the value of β to 2, according with the value proposed by Boulanger et al. (1996). The temperature of

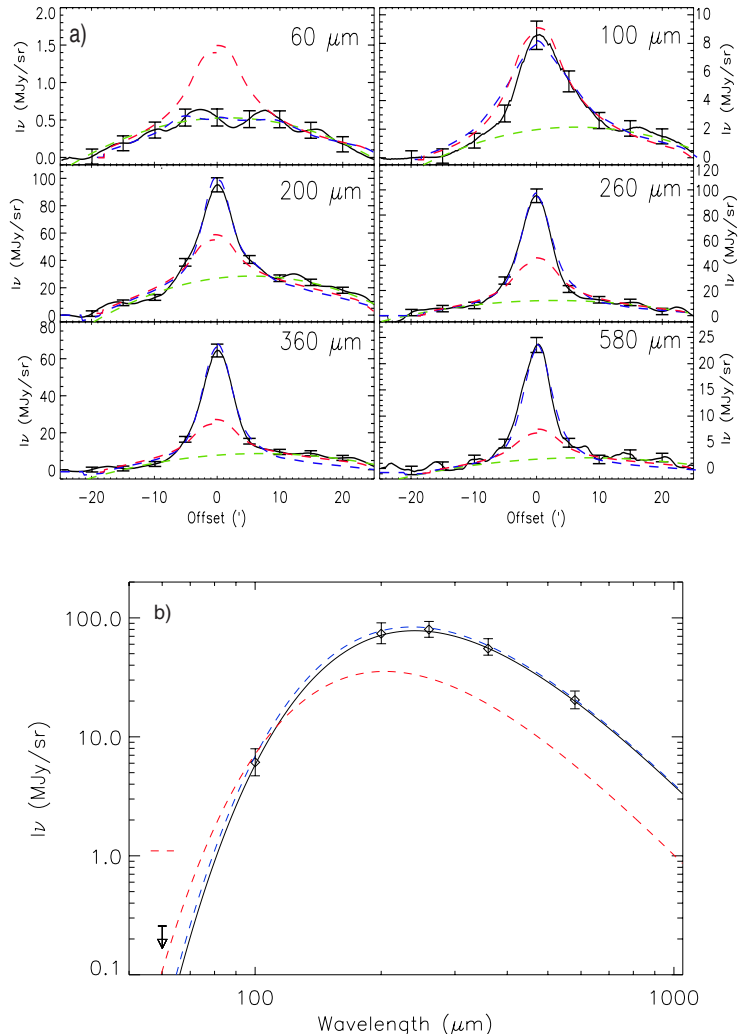


Figure 2. Upper panel presents brightness profiles of the clouds. Lower panel presents spectra of the central position of the filament from which we have subtracted the emission of the surrounding envelope (green dashed lines in upper panel). The data are represented by the black continuous lines in upper panel and by the diamonds in lower panel, with the 1- σ error bars. The standard model (see Sect. 3.3) is represented by red dashed lines. The non-standard model (see sect. 3.4) is represented by blue dashed lines.

the large structure surrounding the filament is determined using DIRBE data at 140 and 240 μm .

Table 1 presents these temperatures measurements.

region	offset	T_{dust}
Filament	0'	$12.0^{+0.2}_{-0.1}$ K
Envelope	8'-25'	14.8 ± 0.6 K
Outside	30'-1°	16.8 ± 0.7 K

Table 1. Values of the dust equilibrium temperature with the incident radiation field at different positions in the cloud.

We have evidenced a significant temperature variation from 16.8 ± 0.7 K outside the cloud to $12.0_{-0.1}^{+0.2}$ K inside the filament. Such a low temperature of 12 K is surprising for a translucent cloud ($A_V \sim 4$). In order to understand its origin we have modelled the filament emission.

3. MODELLING THE FILAMENT EMISSION

3.1. DENSITY PROFILE FROM STAR COUNTS

In order to model the submillimeter emission of our filament, we need an independent tracer of the total dust column density across the cloud. We have used the 2MASS J band star catalog, and applied the star counts method developed by Cambresy (1999) to compute an A_V map. From the A_V profile, we have computed the density profile of the filament. We have decomposed the A_V profile in a large-scale component with a constant extinction value $A_V^{\text{large-scale}}$ (0.5) due to the diffuse medium surrounding the filament, and in the filament itself characterised by an extinction depending on the distance from the centre, $A_V^{\text{filament}}(r) = n_0 \cdot \left(\frac{r}{r_c}\right)^{-2}$, with $n_0 = 5800 \text{ cm}^{-3}$ and $r_c = 2.3'$.

3.2. RADIATIVE TRANSFER

We have used the 3D radiative transfer code developed by Bernard et al. (1992) and improved by Le Peintre et al. (2001). This model computes the distribution of grain temperature and the IR emission of an interstellar cloud. We assume that the incident radiation field is isotropic. We adopt the average interstellar radiation field (ISRF) of Mathis et al. (1983) attenuated by the visual extinction $A_V^{\text{large-scale}}$ (see Sect. 3.1). In order to take the filamentary shape of the cloud into account, we have assumed a cylindrical geometry in our calculation. The dust extinction and emission is computed using the Desert et al. (1990) algorithm. It is a self-consistent model, which takes full account of the transiently-heated small grains. Moreover, our simulations are independent of the gas-to-dust ratio used, because star count measurements give the total quantity of dust on the line of sight, and the radiative transfer code uses directly the dust density inside the cloud.

3.3. RESULTS USING STANDARD DUST

In a first step we have assumed constant optical properties of the dust through the cloud. We have used the standard dust composition adopted by Desert et al. (1990). Fig. 2 compares the model with the observations. The emission of the envelope is properly reproduced (offsets greater than $7'$), but the filament emission (offsets smaller than $7'$) is not well-reproduced by the model. Inside the filament, at wavelengths longer than $100 \mu\text{m}$, the observed emission shows an excess compared to the model, and the grains are too warm inside the densest parts of the filament. This is illustrated by comparing the spectra at the central position of the filament. We have observed a

temperature of 12 K (see Sect. 2.3), while the computed spectrum predicts 14.2 K. Moreover, at $60 \mu\text{m}$, the model presents an emission which is definitely not observed.

In order to reproduce the observations, one solution may be to change both the incident radiation field and the A_V profile inside the observational constraints. These changes does not reproduce neither the observations. Therefore, we conclude that it is the grain properties change inside the filament.

3.4. RESULTS USING NON-STANDARD DUST

In a second step, we have investigated changes in the dust properties inside the filament in order to reproduce our data. We have seen that the model predicts more emission at $60 \mu\text{m}$. The $60 \mu\text{m}$ emission is mainly due to particles not in thermal equilibrium with the radiation field (VSGs for Very Small Grains). Therefore, we suggest that the relative abundance of these particles strongly decreases in the filament. Moreover, the model predicts less emission in the submillimeter range than the one we have observed. A straightforward explanation is to increase the emissivity of grains at thermal equilibrium with the radiation field (BGs for Big Grains). In order to reproduce the data we have realised the following changes:

- The BG emissivity is increased by a factor of $3.4_{-0.7}^{+0.3}$.
- The VSG abundance is decreased by a factor 0.1 ± 0.1 .
- The BG and VSG properties are modified in the same area $4' \pm 1'$, which correspond to an A_V threshold value of 2.1 ± 0.5 .

This simple cloud model in two dust phases separated by an abrupt transition reproduces very well our data (see Fig. 2). We do not resolve the transition area with our data. We conclude that we have evidenced the presence of non-standard dust inside the filament and the spatial correlation of the changes of the BG and VSG properties.

4. DISCUSSION

Several processes may affect the optical properties of dust in dense clouds: ice or molecular mantle formation on grains, coagulation of grains (e.g. Draine 1985).

Preibisch et al. (1991) have shown that ice and carbon mantles on BGs does not increase significantly the submillimeter emissivity. Therefore, we conclude that mantle formation cannot be the main explanation for our observations.

Dust coagulation is efficient for producing large fluffy aggregates (Weidenschilling & Ruzmaikina 1994, Ossenkopf 1993). The optical properties of fluffy aggregates formed by such a process have been computed by several authors (Bazell & Dwek 1990, Stognienko et al. 1995). The submillimeter emissivity of these aggregates strongly increases with fluffiness. At $200 \mu\text{m}$ this increase is typically a factor of 1.5-3.5 for silicate aggregates and 3-20 for carbon aggregates (e.g. Stognienko et al. 1995). On the other hand,

the UV, visible and near-IR absorptivity are not significantly modified (Bazell & Dwek 1990), which implies a decrease of the dust equilibrium temperature with the incident radiation field. Therefore, grain-grain coagulation can explain both the increase of the submillimeter emissivity, and the cold temperature observed. Dynamics simulations (Weidenschilling & Ruzmaikina 1994, Ossenkopf 1993) have shown that, in the physics conditions of the Taurus filament, the coagulation timescale is smaller than the cloud life times. Moreover, the smallest grains (VSGs) coagulate faster than the larger ones (Ossenkopf 1993). Therefore, grain-grain coagulation can explain the huge decrease of the VSG abundance observed even in a translucent cloud.

Finally, we conclude that grain-grain coagulation into fluffy aggregates can produce strong variations of the relative abundance and optical properties of dust observed in our Taurus filament, and certainly occurs in the Taurus filament.

Other observations have also evidence a change in the dust properties. Bernard et al. (1999) observed a low BG equilibrium temperature toward a high latitude cirrus cloud (MCLD 123.5+24.9), presenting a strong deficit of its 60 μm emission. We have tested that an enhancement of ~ 3 the submillimeter emissivity inside this cirrus produce the temperature observed. On larger scales, recently Cambresy et al. (2001) decomposed the far-infrared flux of the Polaris Flare into a cold and a warm component defined by the $I_{60\mu\text{m}}/I_{100\mu\text{m}}$ flux ratio, following the method of Lagache et al. (1998). The comparison of the far-infrared cold component with extinction maps derived from star counts indicates an enhancement of the far-infrared emissivity by a factor of 2-3. Therefore, these observations indicate that in our galaxy the 60 μm deficit seems to be associated with grain submillimeter emissivity enhancements. These two phenomena are probably general effects in the denser parts of the interstellar molecular clouds, which are the signature of dust evolutions in the ISM.

5. CONCLUSIONS

From PRONAOS/SPM data, IRAS data and extinction measurements, coupled with a radiative transfer model, we have shown that the dust properties change in a translucent filament. In one Taurus filament we have evidenced the presence of non-standard dust inside the filament, which appears for a threshold value of $A_V = 2.1 \pm 0.5$. This non-standard dust is characterised by:

- 80-100% deficit of the transiently heated grains (VSGs).
- Increase of the ratio of grain submillimeter emissivity on grain extinction in J band by a factor $3.4^{+0.3}_{-0.7}$.

These changes of dust properties explain the effects observed towards the filament studied:

- Deficit of 60 μm emission.
- Increase of the submillimeter emission.

- Cold equilibrium temperature of the BG with the radiation field (12 K), for a translucent cloud ($A_V \sim 4$).

Grain-grain coagulation processes can produce the relative abundance and the grain optical properties measured for this non-standard dust. Moreover, coagulation timescales ($< 10^6$ yr) are compatible with this scenario in the physical environment of this Taurus filament. Therefore, we conclude that we have evidenced the signature of grain-grain coagulation into fluffy aggregates.

FIRST would be the appropriate instrument to analyse the transitions zone between standard and non-standard dust in order to understand the physical processes involved in the dust evolution that we have evidenced.

ACKNOWLEDGEMENTS

We are indebted to the French space agency CNES who supported the PRONAOS/SPM project. We are very grateful to the PRONAOS/SPM technical team in CNRS and in CNES. This publication makes use of data products from the Two Micron All Sky Survey. We thank the 2MASS team for their work.

REFERENCES

- Abergel A., Boulanger F., Mitzuno A., et al., 1994, *ApJ* 423, 59.
- Bazell D. & Dwek E., 1990, *ApJ* 360, 142.
- Bernard J.-P., Boulanger F., Désert F.X., et al., 1992, *A&A*, 263, 258.
- Bernard J.-P., Abergel A., Ristorcelli I., et al., 1999, *A&A*, 347, 640.
- Boulanger F., Falgarone E., Pujet J.-L., et al., 1990, *ApJ* 364, 136.
- Boulanger F., Abergel A., Bernard J.-P., et al., 1996, *A&A* 312, 256.
- Cambresy L., 1999, *A&A* 345, 965.
- Cambresy L., Boulanger F., Lagache G., et al., 2001, submitted to *A&A*.
- Désert F.-X., Boulanger F., Pujet J.-L., 1990, *A&A* 237, 215.
- Draine B.T. & Lee H.M., 1984, *ApJ* 285, 89.
- Draine B.T., 1985, in *From protostars & Planets II*, Eds. Black D.C., 621.
- Lagache G., Abergel A., Boulanger F., et al., 1998, *A&A* 333, 709.
- Lamarre J.-M., Pajot F., Torre J.-P., et al., 1994, *IR Phys. Tecno.*, 35, 277.
- Laureijs R. J., Clark F. O., Prusti T., 1991, *ApJ* 371, 602.
- Le Peintre F., 2001, et al., in prep.
- Mathis J. S., Mezger P. G., Panagia N., 1983, *A&A* 267, 119.
- Ossenkopf V., 1993, *A&A* 280, 617.
- Preibisch T., Ossenkopf V., Yorke H.W., et al., 1993, *A&A* 279, 577.
- Stognienko R., Henning T., Ossenkopf V., 1995, *A&A* 296, 797.
- Weidenschilling S.J. & Ruzmaikina T.V., 1994, *ApJ* 430, 713.